

ASCA Observations of GX 354-0 and KS 1731-260

T. Narita¹, J.E. Grindlay

Harvard-Smithsonian Center for Astrophysics, Cambridge, MA 02138, USA

and

D. Barret

Centre d'Etude Spatiale des Rayonnements, Toulouse Cedex 04, France

ABSTRACT

We report on ASCA observations of the low mass X-ray binaries GX 354-0 and KS 1731-260. The spectrum of GX 354-0 is best described as a power-law or a Comptonized spectrum with $kT \approx 5$ and $kT \approx 8$ keV and a residual at ≈ 6.5 keV. The residual may be a disk reflection or a Compton broadened Gaussian line from the hot inner ADAF-like coronal region. The absorption column density to the source is $2.9 \times 10^{22} \text{ cm}^{-2}$. No soft thermal component was detected. The spectrum from KS 1731-260 is softer and it is best fit with a two component model with a column density of $1.1 \times 10^{22} \text{ cm}^{-2}$. The likely interpretation is emission from a Comptonizing cloud with an optical depth > 12 and either a neutron star or a disk blackbody emission. We discuss the likely location of the Comptonizing cloud for both sources within the context of several proposed emission models.

Subject headings: X-ray: stars – accretion: accretion disks – stars: individual: GX 354-0, KS 1731-260 – stars: neutron

1. Introduction

The X-ray emission process from low-mass X-ray binaries (LMXBs) is thought to depend primarily on the accretion flow structure and its interaction with the compact object. Early observations showed that several high luminosity sources could be fit with a two component blackbody and disk blackbody model (Mitsuda et al., 1984, White, Stella & Parmar 1988). However, low luminosity sources could be described with either a single component model, such as a power-law or thermal Bremsstrahlung (see White, Nagase & Parmar 1993 and references therein), or two component models involving a harder component and a softer blackbody (Callanan et al. 1995). In an attempt to describe the emission process, White et al. (1985) described that

¹tnarita@cfa.harvard.edu

the thermal Bremsstrahlung-like component in the spectrum of Sco X-1 was due to an unsaturated Comptonization of accretion disk photons in the corona. Previously, a saturated Comptonization model had also been used to explain the hard X-ray emission from Cyg X-1 (Sunyaev & Titarchuk 1980). Recent observations of LMXBs with the broad-band detectors on Rossi X-ray Timing Explorer (RXTE) and BeppoSAX have confirmed that in addition to a hard Comptonized emission, an additional soft thermal component is indeed present in many low luminosity LMXBs (Guainazzi et al. 1998, Barret et al. 1999, Piraino et al. 1999, Barret et al. 2000, Böser et al. 2000). It now seems likely that many X-ray binaries possess both a hard and a soft component in their spectrum regardless of the luminosity. In this paper, we continue the study of the spectra of low luminosity LMXBs by examining two X-ray bursters, GX 354-0 and KS 1731-260. Our intent was to use the higher spectral resolution of ASCA to measure the absorption column to the sources, and to constrain the spectral shape so that we may further study the origin of the emission source.

GX 354-0 (also MXB 1728-34) and KS 1731-260 are Atoll LMXBs (Hasinger & van der Klis 1989) located in the galactic bulge. Of the two, GX 354-0 is the better studied, particularly since its discovery as a burst source (Lewin 1976, Homan et al. 1976). Previous observations of GX 354-0 with Einstein, EXOSAT, Ginga, and ROSAT have shown a spectrum that can be fit with either a thermal Bremsstrahlung of $kT = 13 - 18$ keV, or a power-law of photon index $1.7 - 2.1$ (Grindlay & Hertz 1981, White et al. 1986, Day & Tawara 1990, Foster et al. 1986, Schulz 1999). The column density is large but uncertain, ranging from 1.5 to $3.5 \times 10^{22} \text{ cm}^{-2}$ (Basinska et al. 1984, Schulz 1999). Most recent observations with RXTE and BeppoSAX have found a spectrum best fit with a Comptonization model with a soft component, and a 6.7 keV iron line (DiSalvo et al. 2000, Piraino et al. 2000).

KS 1731-260 was discovered as a transient burster (Sunyaev 1989), but it has since been observed as a persistent source by GINGA, ROSAT, SIGMA, and RXTE (Yamauchi & Koyama 1990, Predehl & Schmitt 1995, Barret et al. 1992, Barret et al. 2000). The Mir-Kvant/TTM observation of KS 1731-260 found a 5.7 keV thermal Bremsstrahlung spectrum absorbed by $2.2 \times 10^{22} \text{ cm}^{-2}$ of neutral hydrogen (Sunyaev 1989). A subsequent ROSAT observation found a power law fit with an N_H of $1.3 \times 10^{22} \text{ cm}^{-2}$ (Barret, Motch, & Predehl 1998). Recent observations by RXTE found the spectrum to be best described by a Comptonized component and a softer thermal component (Barret et al. 2000).

The distance estimates to GX 354-0 range from 4-14 kpc (Grindlay & Hertz 1981), although van Paradijs (1978) estimated a distance to the source of 4.2 ± 0.2 kpc assuming the maximum X-ray burst flux was Eddington limited for a $1.4 M_\odot$ object. RXTE observed a burst with photospheric radius expansion from KS 1731-260, from which Smith et al. (1997) derived a distance of 8.3 ± 0.3 kpc assuming a $1.4 M_\odot$ neutron star. In this paper, we use the distances of 4.3 kpc and 8.3 kpc for GX 354-0 and KS 1731-260. Both sources, being near the Galactic center, are heavily reddened and no optical counterparts have been found. The possible reddened globular cluster identification for GX 354-0 reported by Grindlay and Hertz (1981) was not confirmed by

more sensitive imaging IR observations (Isaacs et al. 1989).

2. Observation and results

GX 354-0 and KS 1731-260 were observed by ASCA on September 27, 1997, with both the SIS and GIS detectors. The total observing time for GX 354-0 was 9 ksec. Nearly half of the observing time was telemetered in the medium and low rates which were saturated due to the relatively high count rate. In this analysis we used the high telemetry mode data to derive the flux estimate, but we combined the high and medium telemetry mode data for the spectral fits. The observing time for KS 1731-260 was 8.5 ksec, and all the data were recorded in the high telemetry mode. No other sources were detected in either observations' field of view.

Initially, we attempted to make the GIS and SIS data consistent. While the GIS residuals from fitting the Crab spectra are only few percent at 2 keV, there is a growing divergence between the GIS and the SIS spectra below 1 keV (ASCA Guest Observer Facility 1999). The quantum efficiency of the SIS detectors has been slowly degrading due to radiation damage, and the current detector calibrations do not account for the loss of efficiency. When we compared the GIS and SIS standard screened data sets (Rev 2) using the latest redistribution matrix and ancillary response files, we found that the flux differed by as much as 15% between the two detectors at energies between 1 to 2 keV and at energies greater than 8 keV. By selecting only the single pixel events (grade 0) in the SIS, we were able to reconcile the high energy discrepancy between the GIS and SIS-1. However, the response of SIS-0 over-predicts the model when only grade 0 events are used (ASCA Guest Observer Facility 1999), and thus we chose to use only the SIS-1 data for further analysis. For the low energy difference, we first tried various extraction diameters for the source, and various extraction regions for the background. Since the SIS-1 local background count rate was < 1% of the source count rate for GX 354-0 and KS 1731-260, this did not affect the spectral shape. Second, we looked for pileup in the SIS-1 data by examining the difference in the spectrum inside and outside the 0.5° source radius. The difference in the best fit spectral parameters for GX 354-0 and KS 1731-260 was within 2%, which indicated that the pileup was not affecting the SIS-1 data. Finally, we used strict screening criteria in ascascreen. Observations only at angles $> 40^{\circ}$ from the bright Earth limb and $COR < 6$ GeV were accepted. However, this also did not modify the low energy spectrum. Other authors have also noted the loss in low energy response from the SIS appearing as an increase in the inferred column density (Hwang et al. 1999, Mukai & Smale 1999). We found that an additional SIS-1 absorption of $4.0 \times 10^{21} \text{ cm}^{-2}$ for GX 354-0, and $2.4 \times 10^{21} \text{ cm}^{-2}$ for KS 1731-260 was required in our observation. To avoid the large systematic error from the uncertain SIS calibration at low energy, we used only the SIS-1 data from 2.0 to 10.0 keV in further joint analysis with the GIS.

We used a standard screening criteria to extract the GIS events. The data were rejected during the time when the Earth limb elevation angle was $< 5^{\circ}$ and during regions of low geomagnetic rigidity (< 4 GeV). The data were also spatially screened for background and calibration events

near the edge, and non X-ray events, as determined from their rise times, were rejected.

2.1. GIS Light curves

We extracted the GIS light curves for both sources and examined them for any temporal variability in the flux. KS 1731-260 did not show any variability exceeding 2%. There was one type-I X-ray burst detected from GX 354-0 but the variability in the remainder of the light curve did not exceed 2%. The All-Sky Monitor (ASM) aboard RXTE showed the flux from GX 354-0 and KS 1731-260 were 90 mCrab and 140 mCrab respectively in the 1.3-12 keV energy band. While the ASM count rate from KS 1731-260 was near the maximum level during the time of our observation, the count rate from GX 354-0 remained at a constant level before and after our observation.

Since the ASM has three energy bands, we plotted the hardness ratio (5.0-12.0/3.0-5.0 keV) for both sources from the time ASM began monitoring each source (Fig. 1). We found the mean hardness ratio of GX 354-0 was larger than that of KS 1731-260, indicating that GX 354-0 generally has a harder spectrum.

From the ASCA data, we also constructed a color-color diagram for the persistent emission from both sources (Fig. 2). We used the GIS-3 data and designated 1.0-3.0 keV for the soft band, 3.0-5.0 keV for the medium band, and 5.0-10.0 keV for the hard band. We did not find strong spectral variability in either observation. Since our observation was short, we cannot comment on the exact position within an Atoll source color-color diagram.

2.2. GX 354-0 X-ray burst

At 23:09:13 UT, a moderate sized type-I X-ray burst was detected from GX 354-0. The satellite was in the high telemetry mode, and the peak count rate in the GIS was 100 cts sec⁻¹. The burst showed an exponential decay with an e-folding time 15 ± 3.5 seconds. In the persistent emission spectral analysis, we excluded the burst data from 23:08:40 to 23:11:20 UT. The deadtime corrected burst data was binned into 6 consecutive time intervals (labeled A-F in Figure 3), and spectral analysis was done on each interval using the combined GIS-2 and GIS-3 detectors (Fig. 4). The persistent emission was used as the background, and the spectra were fit using a simple blackbody model (BB) with neutral absorption. The BB temperature and normalization were allowed to vary, but the column density was fixed at the value derived from the persistent emission fits. The best-fit parameters are listed in Table 1. The BB temperature peaked at 2.1 keV, and the normalization increased asymptotically. No evidence of photospheric expansion was seen. If a 4.3 kpc distance to the source is assumed, the BB radius increased from 1 km to 10 km in roughly 10 seconds and remained at 10 km radius for the next 20 seconds. The peak flux was 1.0 × 10⁻⁸ ergs s⁻¹ (1-10 keV), which corresponds to a luminosity of 2 × 10³⁷ ergs s⁻¹ at 4.3 kpc.

2.3. Persistent emission spectral analysis

2.3.1. GX 354-0

The spectrum from GX 354-0 was analyzed by simultaneously fitting the high and medium telemetry mode data for the GIS-2, GIS-3, and SIS-1 detectors. The GIS photon extraction region was limited to the standard 6° radius centered on the source, and the background was taken from an annulus with an inner diameter of 6° and an outer diameter of 12° . The energy range was restricted to 0.8-10.0 keV band. After deadtime correction, the effective observation time was 6370 seconds. The high telemetry mode source count rates after background subtraction were 23.03 ± 0.07 and $28.12 \pm 0.08 \text{ s}^{-1}$ for the GIS-2 and GIS-3 detectors. The spectrum was binned using grppha with a minimum of 400 counts per bin. The SIS source extraction region was 3.26° and the background was combined from various regions in the detector field of view. The energy range was restricted to 2.0-10.0 keV. The effective observation time was 7582 seconds, and the background subtracted source count rate was $11.46 \pm 0.06 \text{ s}^{-1}$ for the high telemetry mode. The spectrum was binned with a minimum of 100 counts per bin. The spectral fits were done using XSPEC v10.0.

We first tried to fit the simultaneous three detector data with a simple absorbed power law or a Comptonization model (ComptST). This resulted in a power law photon index of $\Gamma = 1.98$ with a $\chi^2 = 1.23$ (1036 dof), or a Comptonizing cloud with an optical depth $\tau = 7.8$ and electron $kT = 5.9$ keV with a $\chi^2 = 1.22$ (1035 dof). The GIS absorption column was $2.90 \times 10^{22} \text{ cm}^{-2}$ for both models. In the residuals, there was an excess at $\sim 6-7$ keV. This excess could not be adequately fit with a high temperature blackbody such as the one found in 4U 0614+091 (Piraino et al. 1999). Adding a Gaussian line ($\chi^2 = 1.05$) or a disk refection component ($\chi^2 = 1.10$) improved the fit. The best fit Gaussian line was broad ($\sim 1.29 \pm 0.30$ keV) with a line centroid of 6.4 keV. The equivalent width of the line was 550 eV. Figure 5 shows the power law fit residuals with and without the Gaussian component. For the disk refection model (PEXRAV), the inclination was fixed to 60 degrees and the abundances were fixed at solar. The refection fraction, which is proportional to the solid angle subtended by the disk at the illuminating source, was allowed to vary. The best fit gave a refection fraction of 2. To see whether a weak soft component was also present, we added a soft blackbody to both the pow+Gaussian and pow+Re models. The χ^2 improvement was only marginal ($\chi^2 < 1$). The standard F-test showed that the addition of the blackbody component was not significant at the 95% confidence level ($F = 0.18$, $\nu = 2$). We list the best fit spectral parameters in Table 2. The total 1-10 keV flux was $2.5 \times 10^9 \text{ ergs cm}^{-2} \text{ s}^{-1}$.

Since the SIS detector has better energy resolution than the GIS, we examined the SIS-1 data alone in the 0.5-10 keV band for additional weak lines. We looked in particular for line features in the residual near 0.7 keV due to ionized Fe or O emissions and the narrow Gaussian line at 1.6 keV reported by DiSalvo et al. (2000). The additional Gaussian components in the model, however, did not improve the fit from the continuum model, and we set an equivalent width upper limit of 17 eV for a ~ 0.05 keV line at 1.6 keV.

2.3.2. KS 1731-260

We used a similar 6° radius GIS source extraction region and a 3.26° SIS-1 source region. The energy band was restricted to 0.8-10 keV band for the GIS and 2.0-10 keV band for the SIS-1. The data were deadtime corrected, and the background was also extracted in a similar manner to GX 354-0. The background subtracted source count rate in the GIS-2 and GIS-3 detectors were 37.05 ± 0.07 and $43.27 \pm 0.07 \text{ s}^{-1}$, while the grade 0 SIS-1 source count rate was $14.76 \pm 0.04 \text{ s}^{-1}$. The total observation time was 7620 seconds and 8772 seconds for the GIS and SIS respectively. The GIS data were also regrouped into spectral bins with a minimum of 1000 counts per bin and 100 counts per bin for the SIS-1.

The simultaneous three detector fit found a much softer spectrum for KS 1731-260. The spectrum was best fit with a combined Comptonization model with a soft thermal component ($\chi^2 = 1.08$; $\nu = 677$). The two component fit (CompST+bb) is shown in Figure 6. From the combined Comptonization and a soft component model, we could not uniquely identify the soft emission as a simple blackbody or a disk blackbody. However, in the CompST+disk model, the ratio of the disk blackbody luminosity to the total luminosity was 0.5, while in the CompST+bb model the blackbody luminosity fraction was only 0.17. A single component Comptonization model ($\chi^2 = 1.37$; $\nu = 679$) or power law model ($\chi^2 = 2.29$; $\nu = 680$) was excluded. A two component model involving a power law and a blackbody was also excluded ($\chi^2 = 1.33$; $\nu = 678$). We list the spectral parameters in Table 3. The total 1-10 keV band flux was $3.20 \times 10^9 \text{ ergs cm}^{-2} \text{ s}^{-1}$, of which the blackbody flux was $0.55 \times 10^9 \text{ ergs cm}^{-2} \text{ s}^{-1}$ and the disk blackbody flux was $1.73 \times 10^9 \text{ ergs cm}^{-2} \text{ s}^{-1}$.

Barret et al. (2000) found a broad iron line in their analysis of RXTE data. Our fits did not require a line, and in Table 3 we report the equivalent width upper limits for a similar ($\nu = 0.8 \text{ keV}$) 6.4 keV iron line (90% confidence). We also did not find any narrow line features at 0.7 keV in the SIS-1 data.

3. Discussion

We observed GX 354-0 and KS 1731-260 in the 1-10 keV energy band and found them to be in very different spectral states. The spectrum from GX 354-0 was best fit with a hard power law ($\nu = 2$) or a hot Comptonization model ($kT = 8-9 \text{ keV}$) with either a broad ($\nu = 1.3 \text{ keV}$) weakly ionized iron line emission or a disk reflection (reflection fraction ~ 2.0). A soft thermal component was not seen from GX 354-0. The spectrum from KS 1731-260 was softer and was best described as a combination of an optically thick Comptonization component and a second blackbody component. The comparison of the derived 1-10 keV flux to other pointed observations (Table 4) showed that ASCA observed GX 354-0 in a relatively low flux state and KS 1731-260 in a middle to high flux state. The corresponding 1-10 keV luminosities of the sources at an assumed distances of 4.3 kpc and 8.3 kpc are 5.2×10^{36} and $2.5 \times 10^{37} \text{ ergs sec}^{-1}$, which are consistent with

the ASM count rate on the day of observation.

With the advances in detector sensitivity, relatively low luminosity LMXBs A-toll sources have been shown to have both a Comptonized emission and a soft thermal emission, like their high luminosity counterparts. The question remains however whether the soft and the Comptonized emissions originate in the same regions regardless of the accretion rate (Barret et al. 2000, Bloser et al. 2000). Mitsuda et al. (1989) found that a multi-color disk and a Comptonizing boundary layer could explain the emission during a high state of 4U 1608-522, but a number of authors have pointed out that the soft thermal component seen in the low state of other A-toll sources could come from either the disk or from an optically thick boundary layer (e.g. White, Stella & Parmar 1988, Guainazzi et al. 1998, Barret et al. 1999, Piraino et al. 1999).

If the Comptonized emission originates in the compact boundary layer and the soft emission comes from the disk, the inferred inner disk radius in KS 1731-260 (~ 10 km) is in good agreement with a canonical neutron star radius. The inner disk temperature of 0.9 keV is also consistent with that observed from 4U 1608-522 and 4U 1820-30 in their high accretion states (Mitsuda et al. 1989, Bloser et al. 2000). For GX 354-0, the lack of soft emission could indicate that the disk truncates at a large radius. If the excess at 6-7 keV is interpreted as an iron fluorescence line, the line energy of 6.4 keV again suggests that the emission is due to the fluorescent emission from the neutral iron in the cool outer disk and not from the hot inner disk.

Alternatively, the Comptonized emission could arise in the extended accretion disk corona (ADC) while the soft component originates near the neutron star surface. For KS 1731-260, the blackbody temperature (0.6 keV) is comparable to the blackbody temperatures found in similar LMXBs (Callanan et al. 1995, Guainazzi et al. 1998, Schulz 1999, Barret et al. 1999, Piraino et al. 1999), but the best fit blackbody radius for KS 1731-260 (24 km) is large for a neutron star. In the case of GX 354-0, an extended ADC subtending a large angle to the disk could result in either a disk reflection component with a large reflection fraction, or a broadened line emission. The best fit value of the reflection fraction is somewhat uncertain since we did not have the high energy coverage to constrain the reflection hump. However, the large disk reflection fraction is similar to the values seen from GS 1826-34 and 4U 1608-522 in their low hard states (Zdziarski et al. 1999). If the excess at 6-7 keV is instead due to the fluorescence emission from the disk, Sunyaev and Titarchuk (1980) found that photons escaping from a Comptonizing cloud will result in an estimated line broadening of $\sim \lambda_c^2$, where λ_c is the Compton wavelength and τ is the optical depth. From the observed line width ~ 1.3 keV we derive an optical depth ~ 4.3 , consistent with the best fit value from GX 354-0.

Our results from KS 1731-260 are best described with a compact Comptonizing boundary layer, and the results from GX 354-0 are seemingly consistent with either of the emission models. However, both models suffer from other observational and theoretical difficulties. In the case of a Comptonizing boundary layer, the hard emission is confined to be near the neutron star surface, $r \sim 10^6$ cm for 1.4 M_\odot neutron star. Yet, in the analysis of dipping LMXBs, the light curve is

best described by a partial covering of an extended corona ($> 10^9$ cm) and a compact soft source (Church et al. 1998). A compact hard emission region would also seem unlikely to produce the broad emission line or the large disk reflection seen from GX 354-0. In the case of an extended Comptonizing corona with an optically thick boundary layer, Sunyaev & Shakura (1986) showed the ratio of the luminosity from the boundary layer should be equal or larger than the luminosity from the corona, if the disk extends to the marginally stable orbit. Yet, the luminosity ratio of the boundary layer to the corona is typically too small (White, Stella & Parmar 1988, Guainazzi et al. 1998, Barret et al. 1999, Piraino et al. 1999). Our observation is no exception; the luminosity ratio of the boundary layer to the corona is only 0.24 for KS 1731-260 and even less for GX 354-0. The energy release in the boundary layer may be reduced if the neutron star spins at near breakup (White, Stella & Parmar 1988), but neither of the neutron stars (GX 354-0 at 363 Hz, Strohmayer et al. 1998; KS 1731-260 at 260 Hz, Wijnands & van der Klis 1997) appear to rotate at speeds close to break up.

Another possible emission mechanism is that the boundary layer may be optically thin during periods of low accretion (Barret et al. 2000). Citing spectral similarities between neutron star LMXBs and black hole LMXBs in their low states, Barret et al. (2000) suggests that an optically thin accretion flow such as an advection-dominated solution of Narayan & Yi (1995) could replace the standard inner disk in LMXBs. If an optically thin accretion flow could transition to the neutron star surface in an optically thin boundary layer, the spectrum would be dominated by Comptonized emission, and only a small fraction of the flux would come from the neutron star surface or the accretion disk (Barret et al. 2000).

In such a scenario, it is plausible that we have observed the interaction of the cold outer disk with the Comptonizing corona in the low accretion state of GX 354-0, namely the 6.4 keV iron line or the reflection from a weakly ionized disk. The broadening of the iron line may be due to the dispersion in the corona if the corona subtends a large solid angle as seen from the disk. At higher accretion rate, the optically thin corona is expected to collapse to an optically thick disk (Narayan & Yi 1995). Correlation of the high frequency quasi-periodic oscillation to the spectral parameters also gives good indication that the disk moves toward the central source during periods of high accretion (Kaaret et al. 1999, Mendez et al. 1999, Böser et al. 2000). One would then expect to observe more emission from the hot ionized disk at higher accretion rate. This is consistent with the 6.7 keV iron line and the 1 keV disk blackbody component reported by DiSalvo et al. (2000) and Piraino et al. (2000) in their observations of GX 354-0 during higher flux states. Similarly, a soft component, in addition to the Comptonizing component, was also observed from KS 1731-260 in its medium and high flux states with ASCA and RXTE. Our observations with ASCA did not find the broad 6.4 keV line that was seen by RXTE, however the upper limit equivalent width set by our ASCA observations is marginally consistent with that found by RXTE. Since the energy resolution of the PCA detector on board RXTE is 18% at 6 keV, it is possible that the broad line seen with RXTE was a superposition of ionized and non-ionized lines. Presumably, such a state would exist during a transitions between the low and

high accretion states, where the emissions from both the outer disk and the inner disk are visible. Further observations using the high resolution gratings on Chandra or XMM may provide more direct evidence on the strength of the line emissions at various accretion rates. Such study should be valuable in constraining the extent of the ADC and its interaction with the accretion disk.

The ASM quick look results were provided by the ASM/RXTE teams at MIT and at the RXTE SOF and GOF at NASA's GSFC. This work was supported in part by NASA grants NAG 5-5103 and NAG 5-5209.

Table 1. GX 354-0 X-ray Burst Spectral Parameters.

Phase ^a	T _{exp} ^b (sec)	CR (sec ⁻¹)		kT _{bb} (keV)		R _{bb} (km)		F _x ^c	χ^2/dof
A	2.44	28.0	4.5	1.81	0.40	3.04	0.97	0.45	17.7/21
B	2.85	63.2	5.4	2.11	0.28	3.72	0.65	1.09	46.2/45
C	3.46	55.1	4.7	1.53	0.11	5.42	0.66	0.71	35.9/49
D	3.10	62.0	5.4	1.15	0.07	9.39	1.16	0.55	38.1/47
E	3.65	45.0	4.5	1.08	0.07	9.48	1.26	0.45	45.4/47
F	11.05	32.7	2.3	0.89	0.04	10.64	1.07	0.23	100.5/113

^aTime interval in burst (cf. Fig. 3)^bDeadtime corrected exposure time^c1-10 keV flux, 10^{-8} erg cm⁻² s⁻¹

Note. | N_H is fixed at 3.1×10^{22} cm⁻². Errors are quoted at 90% confidence level for one interesting parameter.

Table 2. GX 354-0 Persistent Emission Spectral Parameters.

	Pow	Pow + ga	Pow + re	Com pST	Com pST + ga	Com pST + re
N_H^a	$2.90^{+0.03}_{-0.03}$ $1.98^{+0.01}_{-0.02}$	$3.09^{+0.07}_{-0.05}$ $2.15^{+0.06}_{-0.05}$	$3.13^{+0.06}_{-0.04}$ $2.24^{+0.03}_{-0.05}$	$2.89^{+0.02}_{-0.02}$	$3.09^{+0.07}_{-0.06}$	$3.16^{+0.05}_{-0.05}$
kT				$5.99^{+41.02}_{-1.22}$ $7.84^{+1.05}_{-6.42}$	$8.93^{+58.73}_{-3.39}$ $5.69^{+1.76}_{-4.47}$	$8.32^{+23.57}_{-3.16}$ $5.55^{+1.74}_{-1.07}$
E		$6.35^{+0.12}_{-0.14}$ $1.29^{+0.33}_{-0.24}$			$6.36^{+0.12}_{-0.14}$ $1.29^{+0.33}_{-0.24}$	
Re ^b			$2.05^{+7.95}_{-1.27}$			$1.85^{+8.15}_{-0.92}$
F_{tot}^c	2.53	2.51	2.53	2.52	2.50	2.53
² (dof)	1.23 (1036)	1.05 (1033)	1.10 (1035)	1.22 (1035)	1.05 (1032)	1.10 (1032)

^aAbsorption column, 10^{22} cm^{-2} ^bReflection fraction hard limit set at 10^cTotal flux 1.0{10.0 keV, $10^{-9} \text{ erg cm}^{-2} \text{ s}^{-1}$

Note. | Errors are quoted at 90% confidence level for one interesting parameter.

Table 3. K S 1731-260 Persistent Emission Spectral Parameters.

	Com pST	Com pST + bb	Com pST + dbb	Pow + bb	Pow + dbb
N_H^a	$1.44^{+0.01}_{-0.02}$	$1.06^{+0.07}_{-0.07}$	$1.08^{+0.01}_{-0.02}$	$1.37^{+0.03}_{-0.03}$	$1.30^{+0.03}_{-0.03}$
kT	$2.24^{+0.06}_{-0.08}$	$1.93^{+0.09}_{-0.09}$	$1.82^{+0.06}_{-0.07}$		
	$12.71^{+0.28}_{-0.30}$	$18.37^{+2.17}_{-1.72}$	$40.59^{+1.1}_{-9.17}$	$2.15^{+0.03}_{-0.03}$	$2.05^{+0.05}_{-0.06}$
kT_{bb}		$0.58^{+0.02}_{-0.01}$	$0.93^{+0.01}_{-0.01}$	$0.85^{+0.03}_{-0.03}$	$1.28^{+0.06}_{-0.06}$
R_{bb}^c		$23.5^{+2.3}_{-2.6}$		$8.69^{+0.88}_{-0.40}$	
$R_{in}^c \cos^c$			$11.9^{+0.6}_{-0.5}$		$4.27^{+0.52}_{-0.46}$
F_{tot}^d	3.20	3.20	3.20	3.20	3.20
F_{bb}^e		0.55	1.73	0.59	1.22
z^2 (dof)	1.37 (679)	1.08 (677)	1.09 (677)	1.33 (678)	1.27 (678)
EW ^f	< 45.7	< 65.4	< 118.0		

^aAbsorption column, 10^{22} cm^{-2} ^bAssumed distance of 8.3 kpc^cTotal flux 1.0{10.0 keV, $10^{-9} \text{ erg cm}^{-2} \text{ s}^{-1}$ ^dBlackbody flux 1.0{10.0 keV, $10^{-9} \text{ erg cm}^{-2} \text{ s}^{-1}$ ^eEquivalent width (eV) upper limit (90% confidence) for a 6.4 keV line ($\tau = 0.8 \text{ keV}$)

Note. | Errors are quoted at 90% confidence level for one interesting parameter.

Table 4. Comparison of Flux with Previously Reported Fits

Detector	Model	Flux ^a	Line Energy ^b	Line Width ^c	Refs
GX 354-0					
BeppoSAX MECS	Comp+bb	4.4	6.7	0.34	1
BeppoSAX MECS	Comp+bb	3.1	6.7	0.5	2
Einstein MPC	TB	2.9			3
ASCA GIS+SIS	Comp	2.5	6.4	1.3	4
KS 1731-260					
RXTE PCA	Comp+bb	8.1	6.4	0.8	5
ASCA GIS+SIS	Comp+bb	3.2			4
Kvant TTM	TB	0.22			6

^a1.0{10.0 keV, 10^{-9} erg cm⁻² s⁻¹

^bline centroid, keV

^cwidth, keV

References. | (1) Piraino et al. 2000, (2) DiSalvo et al. 2000, (3) Grindlay & Hertz 1981, (4) This paper, (5) Barret et al. 2000, (6) Sunyaev 1990

R E F E R E N C E S

- ASCA Guest Observer Facility. 1999, Data Analysis Software and Documentation (Greenbelt, MD : NASA / G SFC)
- Barret, D . et al. 1992, ApJ, 394, 615
- Barret, D ., Motch, C ., and Predehl, P . 1998, A & A , 329, 965
- Barret, D ., Motch, C ., and Predehl, P . 1998, A & A , 329, 965
- Barret, D ., Grindlay, J.E ., Harnus, I.M ., and Olive, J.F . 1999, A & A , 341, 789
- Barret, D ., Olive, J.F ., Boirin, L ., Skinner, G.K ., Done, C ., and Grindlay, J.E . 2000, ApJ, 533, 329
- Basinska, E.M ., Lewin, W . H . G ., Sztajno, M ., Cominsky, L.R ., and Marshall, F.J. 1984, ApJ, 281, 337
- Bloser, P.F ., Grindlay, J.E ., Kaaret, P ., Zhang, W ., Smale, A.P ., and Barret, D . 2000, ApJ, in print
- Boyle, C.B ., Fabian, A.C ., and Guilbert, P.W . 1986, Nature, 319, 648
- Callanan, P.J., Penny, A.J., and Charles, P.A . 1995, MNRAS, 273, 201
- Claret, A . et al. 1994, ApJ, 423, 436
- Church et al. 1998, A & A , 338, 556
- Cook, W.R . et al. 1991, ApJ, 372, L75
- Day, C.S.R ., and Tawara, Y . 1990, MNRAS, 245, 31
- DiSalvo, T ., Iaria, R ., Burderi, L ., and Robba, R . 2000, A & A , in print
- Fabian, A.C ., Rees, M.J., Stella, L., and White, N.E . 1989, MNRAS, 238, 729
- Foster, A.J., Ross, R.R ., and Fabian, A.C . 1986, MNRAS, 221, 409
- Grindlay, J.E ., et al. 1980, ApJ, 240, L121
- Grindlay, J.E ., and Hertz, P . 1981, ApJ, 247, L17
- Guainazzi, M ., Parmar, A.N ., Segreto, A ., Stella, L ., DalFiume, D ., and Oosterbroek, T . 1998, A & A , 339, 802
- Hasinger, G . & van der Klis, M . 1989, A & A , 225, 79
- Hirano, T ., Hayakawa, S., and Nagase, F . 1987, PASJ, 39, 619

- Ho man, J.A ., Lew in, W .H .G ., Doty, J., Heam, D .R ., and Clark, G .W . 1976, ApJ, 210, L13
- Ho man, J.A ., Com insky, L ., and Lew in, W .H .G . 1980, ApJ, 240, L27
- Hwang, U ., et al. 1999, ApJ, 516, 604
- Isaacman, R . & van Paradijs, J. 1989, A & A , 222, 129
- Kaaret, P ., Piraino, S ., Blosser, P.F ., Ford, E.C ., Grindlay, J.E ., Santangelo, A ., Smale, A.P ., & Zhang, W . 1999, ApJ, 520, L37
- Kallman, T ., and White, N.E . 1989, ApJ, 341, 955
- Ko, Y . and Kallman, T . 1994, ApJ, 431, 273
- Lew in, W .H .G . 1976, IAU Circ., 2922
- Mendez, M ., van der Klis, M ., Ford, E.C ., Wijands, R ., & van Paradijs, J. 1999, ApJ, 511, L49
- Mitsuda, K ., et al. 1984, PASJ, 36, 741
- Mitsuda, K ., Inoue, H ., Nakamura, N ., and Tanaka, Y . 1989, PASJ, 41, 97
- Mukai, K ., and Smale, A.P . 1999, ApJ, 533, 352
- Narayan, R ., and Yi, I. 1995, ApJ, 452, 710
- Predehl, P ., and Schmitt, J.H.M.M . 1995, A & A , 293, 889
- Piraino, S ., Santangelo, A ., Ford, E.C ., and Kaaret, P . 1999, A & A , 349, L77
- Piraino, S ., Santangelo, A ., and Kaaret, P . 2000, A & A , submitted
- Schulz, N .S. 1999, ApJ, 511, 304
- Smith, D.A ., Morgan, E.H ., and Bradt, H . 1997, ApJ, 479, L137
- Strohmayer, T.E ., Zhang, W ., Swank, J.H ., and Lapidus, I. 1998, ApJ, 503, L147
- Sunyaev, R.A . & L.Titarchuk 1980, A & A , 86, 121
- Sunyaev, R.A . 1989, IAU Circ., 4839
- Sunyaev, R.A . 1990, Sov. Astr. Lett., 16, 59
- Swank, J.H . et al, 1977, ApJ, 212, L73
- van der Klis, M ., Stella, L, White, N ., Jansen, F ., and Parmar, A.N . 1987, ApJ, 316, 411
- van der Klis, M ., Hasinger, G . 1989, ApJ, 316, 411

- van Paradijs, J. 1978, *Nature*, 274, 650
- White, N. E., Peacock, A., and Taylor, B. G. 1985, *ApJ*, 296, 475
- White, N. E. et al., 1986, *MNRAS*, 218, 129
- White, N. E., Stella, L., and Parmar, A. N. 1988, *ApJ*, 324, 363
- Wijnands, R., and van der Klis, M. 1997, *ApJ*, 482, L65
- Yamauchi, S., and Koyama, K. 1990, *PASJ*, 42, L83
- Zdziarski, A. A., Lubinski, P., and Smith, D. A. 1999, *MNRAS*, 303, L11

Fig. 1. | RXTE/ASM hardness ratio ($5\text{--}12\text{ keV} / 3\text{--}5\text{ keV}$) of GX 354-0 and KS 1731-260 from MJD 50083 (1/1/96). The observation date is marked with an arrow. The dotted line shows the weighted mean of the hardness ratio since ASM began monitoring each source. The spectrum from KS 1731-260 is typically softer than the spectrum from GX 354-0. The spectrum from KS 1731-260 may be particularly soft on the day of our observation.

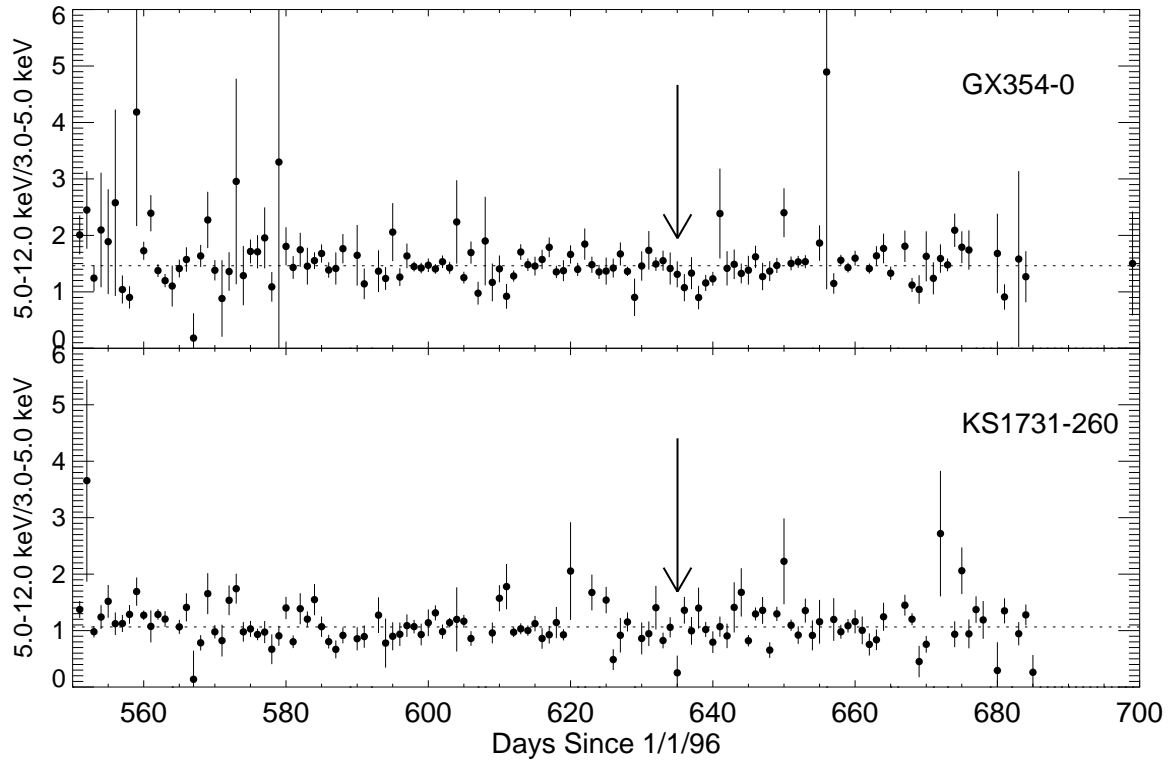
Fig. 2. | The color-color diagrams for GX 354-0 and KS 1731-260 computed from the GIS-3 data. The high and medium telemetry data on GX 354-0 are combined. Neither source showed spectral variations during the pointed observation.

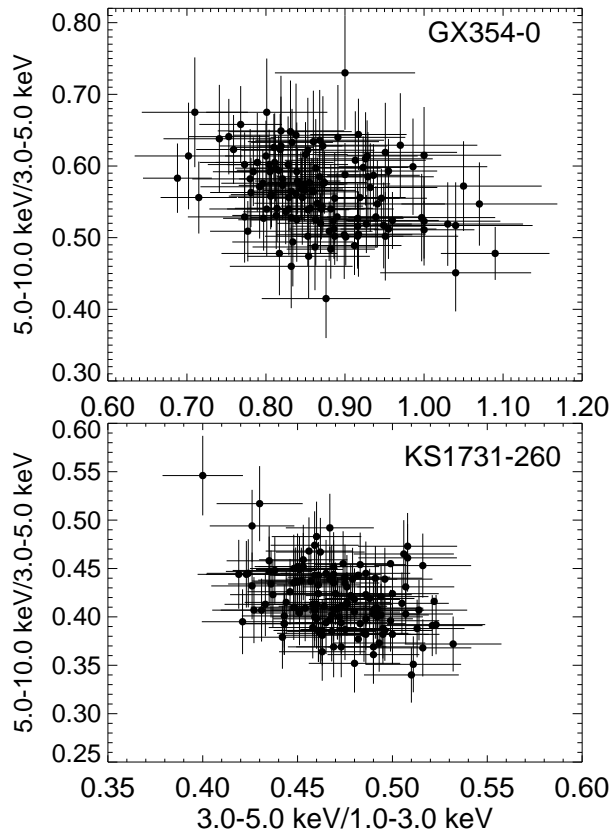
Fig. 3. | A type I X-ray burst light curve from GX 354-0 seen by the GIS-3 detector. The data was binned in 0.5 second intervals, and the burst was subdivided into 6 time resolved segments (A-F) for spectral analysis.

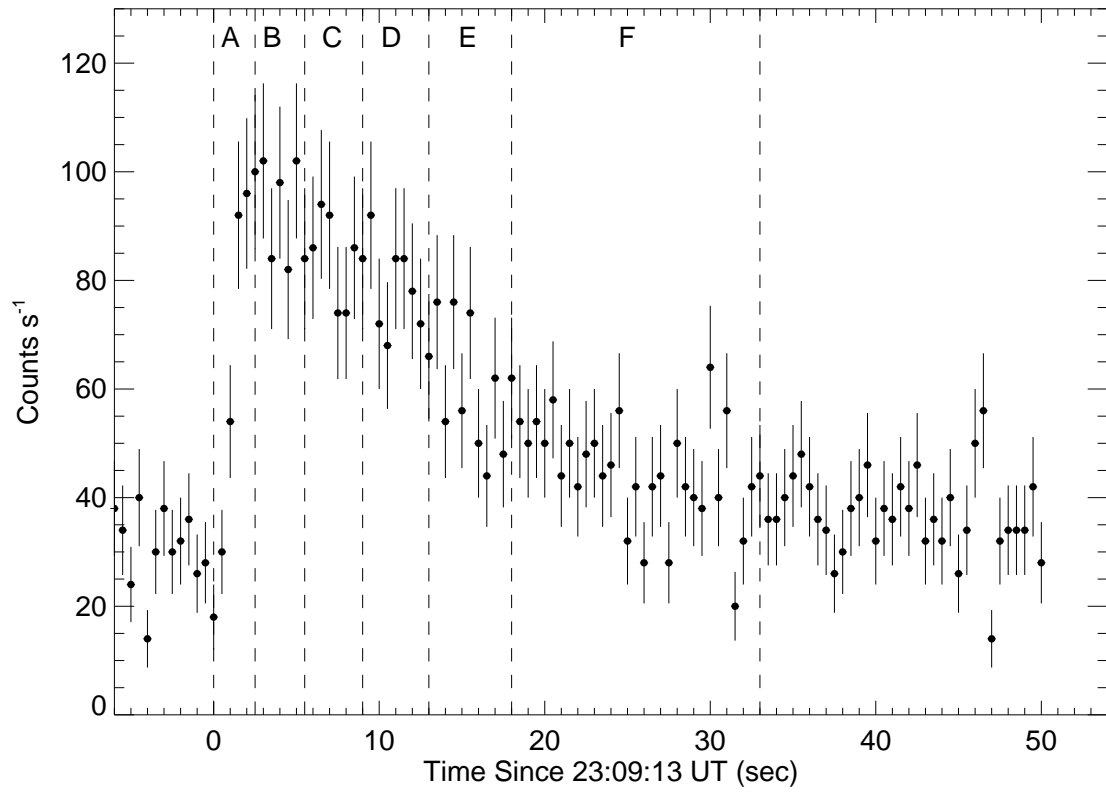
Fig. 4. | The time evolution of the spectral parameters during the X-ray burst. The parameters were derived from simultaneous fits of the GIS-2 and GIS-3 detectors. The absorption column density was fixed at $3 \times 10^{22}\text{ cm}^{-2}$, the best fit absorption from the persistent emission analysis.

Fig. 5. | The GIS and SIS-1 spectra of GX 354-0 simultaneously fit with the power-law + Gaussian model. For clarity, only the high telemetry data is shown. The top panel shows the raw count rate spectrum with the fitted model folded through the instruments' responses, the second panel shows the residuals of the fit, the third panel shows the residual without the additional Gaussian component, and the bottom panel shows the unfolded spectrum with the individual model components. The dot-dashed line is the Gaussian, and the dashed line is the power-law model.

Fig. 6. | The GIS and SIS-1 spectra of KS 1731-260 simultaneously fit with the ComptST + BB model. The top panel shows the raw count rate spectrum with the fitted model folded through the instruments' responses, the middle panel shows the residuals of the fit, and the bottom panel shows the unfolded spectrum with the individual model components. The dotted line is the blackbody, and the dot-dashed line is the ComptST model.







{ 21 {

